A multi-scale statistical description of stacks of non-cohesive thin particles

François Mahé, Christophe Binetruy, Suresh Advani, Julien Ferec, Benedikt Eck

Version of Record: https://www.sciencedirect.com/science/article/pii/S0032591021009864
Manuscript_a6c747aab64b0faf32a538a8811124df

A multi-scale statistical description of stacks of non-cohesive thin particles

François Mahé[a,*], Christophe Binetruy[a,b], Suresh Advani[b,a], Julien Férec[c], Benedikt Eck[d]

[a] *Centrale Nantes, Research Institute in Civil Engineering and Mechanics (GeM), UMR CNRS 6183, 44321 Nantes Cedex 3, France*
[b] *Department of Mechanical Engineering, University of Delaware, Newark, Delaware 19716, USA*
[c] *Univ. Bretagne Sud, UMR CNRS 6027, IRDL, F-56100 Lorient, France*
[d] *Faurecia, 14 Rue des Petits Bois, 35400 Saint-Malo, France*

Abstract

In this article, we provide a general description of a random stack of solid particles. We consider fine particles of any shape distributed evenly on a flat surface. The angular distribution of the particles is arbitrary. In the absence of constraints imposed on the medium, the volume fraction is expressed analytically according to the parameters of the problem. We thus define a generalized strain measurement of the medium taking into account the internal reorganizations of the microstructure which can then be used in analytical mechanical models to predict their response. The approach is verified digitally by generating digital stacks of fibers, disks and rectangular particles.

Keywords: microstructures, layered materials, porous material, probability and statistics, equation of state

*Corresponding author
Email address: francois.mahe@ec-nantes.fr (François Mahé)

1. Introduction

Discontinuous composites are widely used in industrial processes due to their low manufacturing costs, good processability and in some cases comparable mechanical properties to those of continuous fiber composites. There is renewed interest in this class of materials due to the development of recycling technologies that rely on grinding to create new discontinuous materials [1, 2, 3]. Discontinuous composites consist of solid particles of finite size immersed in a flexible matrix and distributed in a random or controlled manner (see Fig.C.1). Depending on the industrial process and the application, these solid particles can be fibers, chopped tows, tapes or platelets [4, 5]. For instance in Sheet Molding Compounds (SMC) or Prepreg Platelet Molded Composites (PPMC), the solid particles are deposited randomly on a flat surface resulting in an architecture which we will refer to as "random stacks". The solid material is mainly layered in the vertical direction that corresponds to the deposition direction. These materials are typically used in molding processes in which the suspension can be highly deformed by mechanical loads applied along the vertical direction. The internal meso-structure is then subjected to major in-plane and through-the-thickness geometric transformations [6, 7, 8, 9, 5]. Since the particles are not cohesive, each particle can move relative to the others changing the microstructure during the molding process. The resulting microstructure will determine the final mechanical performance [10]. It is generally acknowledged that this complex deformation behavior is governed by the mechanical properties of the meso-structure [8, 11, 12] and the particle to particle interaction mechanisms [13] that affect their displacements (such as frictional forces for compact systems or hydro-

dynamic interactions in the case of suspensions). The industrial use of these materials is limited as accurate descriptions of their transformation during the molding process are not available. In the absence of such understanding it is difficult to control part to part variability during the molding process.

It has been shown that the mechanical response of a bed of packed fibers under through-thickness compression is non-linear and depends on geometrical parameters such as fiber volume fraction, initial fiber orientation and fiber curvature [14, 15, 16]. In the absence of a matrix phase, there is no relative displacement between the fibers during the compression. Van Wyk's law relates the compression pressure due to the elastic contribution of the fibers to the fiber volume fraction [17]:

$$P \propto \phi^n - \overline{\phi}^n \tag{1}$$

where P is the compression pressure, ϕ is the volume fraction of the fibers and n is the exponent which depends on the material and takes a value generally between 3 and 5, depending on the deformation modes of the fiber. This expression also introduces $\overline{\phi}$, which is equal to zero for continuous fibers (i.e. with an infinite aspect ratio) and corresponds to the fiber volume fraction when no compression force is applied (in an elastic dry system). We will refer to this state as the "bulky" configuration, which is also referred to in the literature as "loose", "unloaded" or "unforced packing" [14]. This value is required to define the appropriate deformation metrics and to obtain mechanical constitutive models. An analytical expression was derived by Toll in [14] to relate the bulky fiber volume fraction to the orientation distribution and the fiber aspect ratio. This theory was then widely used in other models to describe the mechanical compression of dry or lubricated fibrous systems

[18, 11].

To understand more precisely the internal structure of random stacks and the bulk mechanical behavior of the arrangement, some authors used numerical generations of packed particles. These algorithms can be classified into two main groups. The first group of techniques is based on the Random Sequential Addition (RSA) algorithm [19]. Particles are successively added in a domain considering the non-penetration between the particles. The placement is determined to reach a targeted volume fraction. This purely geometrical method allows one to obtain digital materials with many particles but it cannot represent physical materials, where the internal contact forces and deformations of the particles govern the internal structure. The second group of methods uses finite elements to generate digital materials [20]. In this case, a large mechanical problem is solved by considering the particle deformations and all solid contacts. This produces realistic and complex composite materials, where different deformation modes are involved (sliding, shear and bending, transverse compression), as it is shown in Fig.C.2. In [5], the authors studied the meso-structure of randomly dropped square platelets to model an industrial molding process. They discussed the complex description of the resulting material for different compaction levels.

In this paper, we present a general analytical method to revisit Toll's description and calculate the solid volume fraction in random stacks of thin solid particles. Then we will discuss these values for different particle geometries and compare them with both experimental and numerical data from the literature. In particular, our description of the bulky configuration will be compared to numerical simulations of random stacks. Then, we will discuss

our modeling assumptions and especially the initial consolidation due to the gravitational force, comparing it to the realistic direct simulation of [5]. We will demonstrate that the proposed model predicts the volume fraction of real materials made of stacked thin particles.

~~Random microstructures are a result of interactions between solid particles in a compliant matrix in industrial processes. In many cases, random microstructures consist of an aggregation of solid particles. Such heterogeneous media can be discontinuous, porous, without internal cohesion, resulting in complex behaviors when they are subjected to external loading. Manufacturing products out of these materials usually induces transformations on several scales that can affect their macroscopic behavior and mechanical response. Natural granular media are a widely studied class of random microstructures. In many cases, industrial precursor materials are created by a random dropping process of solid particles on a planar surface where they stack up and form a layered structure. This type of precursor material microstructure is formed in various industrial processes which involve short fiber suspensions and composites, recycling of composites, paper industry, textiles, filters, biology, chemistry, etc. [21, 11, 4, 22, 12, 1, 3, 23, 24]. We will call this class of microstructure "random stacks". Precursor materials are used as initial materials in industrial processes to form useful products by subjecting them to mechanical loadings such as transverse compression. The resulting final microstructure is a function of the initial random stack microstructure hence modeling approaches require appropriate descriptions of these precursor materials. The objective of this approach is to get a physical representation of the microstructure of these materials, which can change significantly during the~~

manufacturing process. These materials encompass fiber or platelet reinforced composite materials. Their use in the manufacture of structural components involves displacement over long distances, which will affect the mechanical response of the final part. The representation of these microstructures is important for modeling the evolution of these materials and for capturing some of the behaviors that cannot be treated by the usual continuum theories.One such random stack is formed by dry fibers. A seminal study about the transverse compression of dry fibers can be found in [17]. It is now established that the mechanical response of a bed of packed fibers under through-thickness compression is non-linear and depends on geometrical parameters such as fiber volume fraction, initial fiber orientation and fiber curvature [14, 15, 16]. When a matrix phase is present, the deformation of the bulk material induces in-plane displacements and local deformations. If the matrix is a viscous fluid, fibers can be advected by the resulting flow of the in-homogeneous suspension. The internal microstructure is then subjected to major geometric transformations [6, 7, 8]. These behaviors were also observed for other types of particles as strands and platelets [9, 5]. The similarity between fibrous systems and granular media may be seen in [25], where the authors give experimental results concerning the particle volume fraction in such random media. Similar mechanical responses are observed in lubricated compression where friction effects play a major role. The mechanical behavior depends on the initial microstructure and its deformation state as it evolves during the transformation. An improved description of the initial microstructure of these random stacks needs to be taken into account to describe their evolution under applied stress and deformation improving our ability to

guide the processing of such materials to steer their microstructure to tailor desired mechanical performance. In this paper, we propose a new approach to describe the microstructure of these random stacks. The model presented in [14] for fibers is generalized to address a broader class of microstructures addressing the stacking of thin particles. Analytical expressions for the volume fraction of different type of solid particles are derived. Then, an equation of state is introduced to describe the deformation state of these media. This law establishes a relation between the different multi-scale transformations that generally occur during forming processes. It provides a general kinematic description which can be used in a mechanical model to describe the response of the microstructure subjected to external loading.

2. Theory

2.1. Modeling assumptions

We focus on a certain class of thin materials such as fibers, fiber bundles or particles that are randomly dropped on a planar surface where they "pile up" and create a layered structure that we call "random stack". A stack is made up of the same particles. This type of microstructure has similarities to granular media, which are also random aggregates of particles, however layered structures require a more complex description [25, 26].

In this study the generation of random stacks relies on four assumptions:

1) Particles are assumed to be of constant thickness, finite dimension and thin as our description of stacks will require a simplification to describe contacts between particles. Contact directions are perpendicular

to the planar surface on which particles are dropped down. It simplifies the formulation, which is not valid for granular media or nested particles. No partial contact nor nested contacts are permitted.

2) Planar orientation distribution is assumed as the particles in a layer lie in the same plane and form a layered stack and hence no interpenetrations are allowed. The planar orientations can be described by a (2D) distribution function.

3) Uniform spatial distribution assumption implies that the particles are dropped without any spatial correlations between particles' positions which leads to statistically homogeneous microstructures.

4) Statistically equivalent layers assumption allows to average quantities over the layers and neglect boundary conditions at the top and bottom of the microstructure.

The resulting microstructure is a layered structure of particles randomly added to the stack. As there is no interpenetration and the distribution is random, particles of a certain length must stack creating internal voids or porosities inside the microstructure. If no loading is applied (no force on boundaries and no body force), the stack lies in an initial uncompressed state referred to as "bulky". In this state, the solid volume fraction is low and we will see that it can be predicted from the geometrical parameters of the problem. Solid volume fractions lower than the bulky volume fraction correspond to "suspended particles", which may be the case if particles are immersed and dispersed in a matrix. If the volume fraction is higher than the bulky volume fraction, this configuration is referred as "compacted stacks".

Firstly, we will only consider unloaded loose stacks. In this paper, quantities related to the bulky state will be noted with an over line symbol.

Finally, particles are assumed to be non cohesive; In-plane transformations are allowed to rearrange the particles within the microstructure. For instance, consider an evolving fibrous microstructure where fibers are aligned during a transformation. It may be due to the presence of a fluid matrix which imposes in-plane drag forces on the fibers. In the same way, a squeeze-flow will transport the fibers in the plane. In-plane forces may be considered to represent friction effects. Conversely, a compression of a fibrous microstructure without internal rearrangements leads to the creation of new contacts between particles, the latter will deform and the vertical loads to compress it further will increase. In our work, we take into account these internal rearrangements which will affect the internal forces thus requiring a new geometric description for random stacks.

2.2. Stacking of straight fibers with an isotropic angular distribution

First, we consider a stack of short, straight fibers. The fibers are of length L and distributed according to an isotropic angular distribution in the plane : $\psi(\theta) = 1/(2\pi)$. When forming the stack, if two fibers intersect, the second will stack on top of the first and end up on the top layer. In the absence of constraints imposed on the medium, the stack consists of successive layers containing fibers and porosities (see Fig. C.3). The characterization of the microstructure is done using the volume fraction of fibers $\overline{\phi} = Nv/V$, where N denotes the number of fibers distributed in the volume V, and v is the volume of a fiber. In the absence of constraints, the stack is said to be "bulky". The stack is in a loose state which maximizes its porosity fraction

by verifying that each fiber rests at least on another or on the deposition surface. Using the assumption that all layers are statistically equivalent, the volume fraction is identical in each layer of the stack and is equal to $\overline{\phi}$. It is then necessary to determine an analytical expression of the density of fibers in each layer of the microstructure by relating it to the probability of intersection between two fibers. ~~Some statistical geometry tools, described hereafter, allows us to establish these models.~~ Statistical geometry tools, described below, are used to build these models.

According to the Crofton's formula [27], if we consider any two curves $\mathcal{C}$ and $\mathcal{C}'$, the number of their intersections is related to their lengths, respectively L and L':

$$\int_{\Gamma} \chi(\mathcal{C} \cap \mathcal{C}') d\Gamma = 4LL' \tag{2}$$

where $\chi(\mathcal{C} \cap \mathcal{C}')$ denotes the number of intersections between the two curves. The integration space $d\Gamma$ represents the set of transformations (translations and rotations) of the two curves, it is the set of possible configurations. This formula indicates that the sum of all possible intersections between the two curves (accounted with all the translations and rotations) represents an area equals to four times the product of lengths. It is demonstrated by first considering two small straight segments of respective lengths $d\ell$ and $d\ell'$. The integral then becomes:

$$\int_0^{2\pi} |\sin(\theta)| d\theta d\ell d\ell' = 4 d\ell d\ell' \tag{3}$$

where θ is the relative angle between the two segments which can take all the values between 0 and 2π. This is the area shown in Fig. C.4 which is integrated between 0 and 2π. Eq.(3) can then be integrated along the two curves in accordance with Crofton's formula Eq.(2).

The area of the configuration space is given by:

$$\int_{\Gamma} d\Gamma = \int_0^{L'} \int_0^{L} \int_0^{2\pi} d\theta d\ell d\ell' = 2\pi L L' \tag{4}$$

We now consider two consecutive layers of the stack of straight fibers of length L. Each fiber of layer #2 rests on at least one fiber of layer #1. By the assumption of equivalence of the layers, it can be considered that the two layers contain the same number of fibers. Two surfaces can be defined from previous relations. We define A as the overlapping area, i.e. the average zone around a fiber allowing crossings with a second fiber present in this zone. It is defined using the Crofton's formula (2)

$$A = \frac{1}{2\pi} \int_{\Gamma} \chi d\Gamma = \frac{2}{\pi} L^2 \tag{5}$$

We also define the area S from Eq.(4)as:

$$S = \frac{1}{2\pi} \int_{\Gamma} d\Gamma = L^2 \tag{6}$$

The intersection probability between two random fibers becomes the ratio of A over S. Then, S is interpreted as the average area which contains only one fiber, or the inverse of the areal density of fiber per layer. Hence, S is directly related to the fiber volume fraction in the bulky state by:

$$\overline{\phi} = \frac{v}{Se} \tag{7}$$

where v and e are the volume and the thickness of a fiber respectively. The analytical value of the fiber volume fraction of the bulky stack is thus obtained: $\overline{\phi} = \dfrac{v}{L^2 e} \propto \dfrac{1}{r}$, where $r = L/w$ represents the fiber shape factor. The value of the multiplicative constant depends on the cross-section of the fibers

and is equal to $\pi/4$ for an elliptical cross-section. Note that the fiber volume fraction only depends on the geometry of fibers in the case of a random stack with an isotropic angular distribution. We also establish the relationship between the two surfaces defined in Eqs. (5) and (6) by the expression (8) which will be generalized later:

$$\frac{A}{S} = \frac{2}{\pi} \tag{8}$$

2.3. Generalization to arbitrary shaped particles

Results in Eqs. (5), (6), (7) and (8) are extended to random stacks of arbitrary shaped particles. We start by considering curved fibers of length L, distributed according to a given angular distribution in the plane ψ. $\psi(\theta)d\theta$ is the probability of finding an element of length along a fiber oriented between θ and $\theta + d\theta$. ψ must fulfill the normality condition $\int_0^{2\pi} \psi(\theta)d\theta = 1$. We can note that the angular distribution is a symmetric function: $\psi(-\theta) = \psi(\theta)$.

We introduce c the average number of contacts between two fibers, which is a function of the curvature of fibers. It is equal to 1 for straight fibers because there is always only one intersection. c is equal to 2 when the fibers form circles and c is equal to 4 when the fibers fold to form a U (as shown in Fig. C.5).

We also define the isotropy factor α by:

$$\alpha = \frac{\pi}{2}\langle \| d\vec{\ell} \wedge d\vec{\ell'} \| \rangle \tag{9}$$

This parameter measures the effect of the angular distribution on the fiber volume fraction. $d\vec{\ell}$ and $d\vec{\ell'}$ are vectors tangent to the fibers and represent the local orientations of fibers. α is equal to 1 for fibers equally distributed

in all directions or randomly curved (Fig. C.6). α is equal to $\pi/4$ for fibers oriented in two random perpendicular directions. α tends towards 0 for straight and parallel fibers (Fig. C.6). ~~Examples of the calculation of these two parameters are given in 5.~~ Solving Jeffery's equation for a population of straight fibers in a planar shear flow allows one to obtain the evolution of α. Its evolution is related to the second invariant of the orientation tensor, which also represents the evolution of relative orientations in the population. The representation of α is a function of the second invariant of A_2 and is shown in Fig. C.7 . Examples of the calculation of c and α are presented in 5.

With the help of these two geometric parameters α and L, Eqs. (5) and (6) can be generalized for any stacks taking into account multiple intersections:

$$Ac = \int_{\Gamma} \psi\chi d\Gamma = \frac{2}{\pi}\alpha L^2 \tag{10}$$

$$Sc = \int_{\Gamma} \psi d\Gamma = \alpha L^2 \tag{11}$$

Eq.(10) allows one to calculate the average area when two fibers intersect (A), while Eq.(11) allows one to calculate S and the areal density of fiber per layer. The derivation of these relationships is given in the 5. The ratio between these two areas always verifies the condition given in Eq.(8).

Noting that the area S contains on average a single fiber, one can combine Eqs. (7) and (11) to obtain the volume fraction of fibers for a stack of fibers in the general case:

$$\overline{\phi} = \frac{cv}{\alpha L^2 e} = \frac{c}{\alpha r} \tag{12}$$

where ~~$r = L/w$~~ $r = L^2e/v$ is the shape factor of fibers. For long fibers, $r \sim L/w$.

Any random fibrous stack can thus be described in its bulky state, i.e., in an unloaded state, using its bulky volume fraction (12). This latter is a function of the geometry of fibers, angular distribution α defined in Eq.(9), and fiber curvature characterized by c, which represents the average number of contacts or crossings between two fibers. Note that according to Eq.(12), c is related in the case of high curvatures (where the convex hull of the curved fiber still has an high aspect ratio) with the fiber length ℓ and the linear length of its convex hull L:

$$c = \left(\frac{\ell}{L}\right)^2 \quad \text{and} \quad \overline{\phi} = \frac{1}{\alpha r}\left(\frac{\ell}{L}\right)^2 \tag{13}$$

considering the product of Eq.(12) with an effective fiber content $\varphi = \frac{\ell w}{LW}$, where w is the fiber width and W is the convex hull width. In Eq.(13), the number of crossings c has the same expression ~~than~~ as the usual definition of the hydraulic tortuosity [28].

It is noteworthy that the previous results remain unchanged during the passage from a curved fiber forming a lace to a particle without a hole surrounded by this same lace. Thus, we see that a stack of particles of any shape is also characterized by the analytical expression (12). Table [C.1] gives the expressions of ~~the~~ bulky volume fractions ~~of stacking of different shapes of particles~~ for different particle shapes. The calculations are detailed in the Appendix B.

2.4. Comments

From the Eq.(12), we can extract some additional results about random stacks. It can be seen that the bulky volume fraction depends both on the occupied area v/e and the length of the fiber or the perimeter of the particle. Thanks to the isoperimetric theorem [29], it can be established that the maximum volume fraction in the absence of constraints corresponds to that of a stack of disks, so $\overline{\phi}_{\max} = 1/(2\pi)$.

Note also that for the case of fibers, the volume fraction diverges for small values of α, which corresponds to aligned fibers. However, the volume fraction must be less than 1. This is due to the fact that in our calculations we have considered fibers as 1D objects, which tends to infinity if they are parallel. We have just seen that the volume fraction cannot exceed the value of $1/(2\pi)$. We can thus establish a domain of validity for the isotropy factor beyond which, the alignment of the fibers requires one to consider the width of the fibers (see the result for the rectangular particles in [C.1]). We obtain:

$$\alpha > \alpha_{\min} = 2\pi \frac{cv}{L^2 e} \propto \frac{2\pi c}{r} \tag{14}$$

For fibers of rectangular section, with an aspect ratio $r = 25$, this corresponds to a limit value $\alpha_{\min} \simeq 0.25$. The corresponding situation is shown in Fig. C.8.

It can be noticed ~~than~~ that the form of the equations in C.1, especially the relation for rectangles is really similar ~~than~~ as the one which is introduced in [30]. The difference comes from the fact that in the real case studied by the authors, the microstructure is not bulky, due to the collapse of the microstructure under the weight of its particles. The same kind of configu-

rations is also studied in [5]. To understand the effect of the collapse of the microstructure, the compaction measurement may be related to the number of contacts per particle n_c. In the bulky state, it is assumed that each particle is in contact (on average) with only two particles, one above and one below. Then, $n_c = 2$ ~~if $\lambda = 1$~~. ~~It seems reasonable to suppose that the number of contact evolves linearly with λ^{-1}.~~ For different values of ϕ, one can reuse the previous geometrical reasoning and the definitions of A and c (Eq. (10)). Then, the number of contacts on a fiber is equal to the number of fibers N which have their center-lines embedded in a volume Ae (where e is the fiber thickness) around the first fiber, multiplied by c, the average number of intersections between two fibers. Introducing the volume fraction ϕ and Eq. (12), it comes:

$$n_c = Aec \times N = \frac{2c}{\pi} \times (\phi/\overline{\phi}) \tag{15}$$

It will allow us to define the compaction as the ratio between $\overline{\phi}$ and ϕ which will be reformulated within a mechanical framework in Eq. (18). Then, the number of contacts per fiber evolves linearly with λ^{-1}. This linear dependence on the volume fraction has already been observed in 3D suspensions [14]. A microstructure compacted twice has an average number of contacts per particle equals to 4. From n_c, the average length between contact points along fibers ℓ_c may be defined as the ratio between the fiber length and $2n_c$. In the case of stacked fibers, it comes:

$$\ell_c = \frac{L\lambda}{2} \tag{16}$$

Then, comparing with results given in [5] and [30], it appears that the studied microstructures are already compacted due to their ~~weigth~~ weight .

2.5. Kinematic equation

The relation (12) also allows one to calculate the average height of random stacking. By noting ϱ the number of particles distributed per unit area, the bulky thickness of the stack is given by:

$$\overline{h} = \frac{\varrho v}{\overline{\phi}} = \frac{\alpha}{c}\varrho L^2 e \tag{17}$$

So far, results have been obtained for stress-free microstructures. That is to say that the stack occupies a maximum volume. We have seen that this unloaded state can be characterized by the bulky volume fraction (12) or the bulky height of the stack (17), which are functions of the geometry, angular distribution and the surface density of the particles. If we consider a transformation of the microstructure causing one of these parameters to vary, the volume fraction and the thickness of the stack will change without however inducing compressive forces in the medium. Imagine such a microstructure in a suspension flow. In the absence of friction, the particles are dragged by the fluid and the thickness of the stack decreases without constraints.

Now consider a fibrous microstructure in a shear flow [31]. The fibers gradually align, which decreases the value of α and increases the volume fraction. In the absence of friction, there are still no stresses induced by these internal rearrangements. It is thus possible to generally define a deformation measurement taking into account the reorganizations of the microstructure for stacks of particles. In a way analogous to classical continuous mechanics, where one defines a stretch compared to a state of reference assumed unloaded, one introduces the parameter of compaction λ defined by:

$$\lambda = h/\overline{h} = \overline{\phi}/\phi \tag{18}$$

where h and ϕ denotes respectively the height and the volume fraction of particles of the stack. $\overline{h}$ and $\overline{\phi}$ always denote the values in the bulky state, free from compression stresses. We can thus re-express (12) and (17) to obtain a kinematic equation connecting the various transformations of the microstructure to the compaction parameter:

$$\frac{h}{\varrho v} = \frac{1}{\phi} = \alpha\lambda\frac{L^2 e}{cv} \tag{19}$$

We can explain the physical meaning of (19) by means of its time derivative:

$$\frac{\dot{h}}{h} - \frac{\dot{\varrho}}{\varrho} = -\frac{\dot{\phi}}{\phi} = \frac{\dot{\alpha}}{\alpha} + \frac{\dot{\lambda}}{\lambda} - \frac{\dot{c}}{c} + \frac{\dot{e}}{e} \tag{20}$$

considering here that L and v are constants. The first two terms on the left hand side represent the vertical compression and the induced flow, the third term represents the consolidation of the material. These terms describe the macroscopic deformations. On the right hand side of the equation, the first term expresses the reorganizations of the microstructure and the second term is the true strain of the medium (that which induces vertical stresses). The last two terms correspond to the deformations of the particles (see Fig. C.9).

A basic application of Eq.(19) allows one to find van Wyk's law for the compression of fibrous systems [17]. Let's consider a stack of straight fibers ($c = 1$). The characteristic distance between contact points may be considered as proportional to the compaction and the fiber length 16. From Eq.(20), the strain increment may be written as:

$$d\varepsilon = \frac{d\lambda}{\lambda} \tag{21}$$

We assume that the fibers bend during the compression. Then, the stiffness of the material may be estimated as inversely proportional to the cube of the

characteristic distance between contact points:

$$K \propto \frac{1}{\ell_c^3} \propto \frac{1}{L^3\lambda^3} \tag{22}$$

The compression pressure P is equal to the applied force on the area $S = \alpha L^2$. If the force is equal to the product of the stiffness (22) and the strain (21), the increment of compression pressure is:

$$dP \propto \alpha^{-1} L^{-5} d(\lambda^{-5}) \tag{23}$$

Applying Eq.(19), it becomes the more classic form:

$$dP \propto \alpha^4 d(\phi^5) \tag{24}$$

which gives after integration the classic form of van Wyk's law:

$$P \propto \frac{1-\lambda^{-5}}{\alpha L^5} \tag{25}$$

$$\propto \alpha^4(\phi^5 - \overline{\phi}^5) \tag{26}$$

where $\overline{\phi}$ is the bulky volume fraction. A more detailed calculation that is not developed here would lead to the coefficient of proportionality which corresponds to the compression modulus of the fibrous material (see [14] for more details about the compression of fibrous media).

A general method is thus obtained for describing the microstructures of fibrous stacks and more generally the random stacks of particles. Thanks to the analytical formula of the bulky volume fraction, we were able to obtain a characterization of the true deformation of the medium (which induces

vertical forces), taking into account the internal reorganizations of the microstructure and the various possible transformations for non-cohesive particles. In the following, the analytical formulas of the volume fraction of different stacks are compared with a numerical approach.

3. Computational modeling

First, we propose a numerical generation algorithm to reproduce random stacks for different particle geometries, with the assumptions used to derive the analytical packing models. The generated microstructures will be compared to real cases from the literature.

3.1. Virtual microstructure generation

A stacking generation algorithm adapted to the studied situations is implemented in Python. A periodic square domain is used to represent an infinite deposition area. N particles are deposited on this domain, with a uniform spatial distribution and a given angular distribution. The angles are taken in the horizontal plane, transverse to the deposition direction. The particles remain in the plane during the entire process. Contacts between particles are calculated for each new particle added to the stack. When a contact is detected, the new particle is added onto the next layer. There is no charge applied, the particles are not subject to gravity force and the stack is in a free unloaded state.

~~A simple stack generation algorithm is implemented in Python in order to generate structures verifying stack modeling assumptions. On a periodic square domain, N particles are deposited according to a uniform spatial distribution and a given angular distribution. The contacts between particles~~

~~are calculated accounting for the periodicity of the domain. Intersections between particles are detected, then, layers are reconstructed considering particle addition order. There are no applied loads, particles have no mass, stacks are in loose unloaded state.~~

Generation parameters are:

- Disks: diameter = 1, thickness = 1, number of disks = 11250 , domain length = 15
- Strands: length = 1, width = 1/2, thickness = 1, number of bundles = 4000, domain length = 10
- Squares: length = 1, thickness = 1, number of platelets = 11250 , domain length = 15

The volume fraction is calculated from the resulting bulky thickness using Eq.(17). Twenty realizations of stacks are generated in each case. The numerical average bulky volume fractions are compared with values predicted from the models reported in Table [C.1]. Results are presented in Fig.(C.11-C.14).

3.2. Comparison with published results

The synthetic microstructure generator and analytical models predict the solid volume fraction in a reference configuration called "bulky state", in which the body forces are ignored. In physical samples, the gravitational force causes a densification of the microstructure.

In our model, in the bulky state, each stiff particle remains in the plane, and has on average two contacts with other particles: one with the upper

particle, and another with a lower particle. Assuming that rigid particles do not deform under body forces, the compaction state depends only on the number and distribution of contacts. In a gravitational field, the solid bodies fall before reaching a stable state in the stack. For a straight fiber, this stable state corresponds to a configuration with two support points per fiber, so on an average, four contact points per fiber (two contacts below, and two contacts above) ~~(see Fig. ??)~~. In the same way, for convex particles, a stable state requires two contact lines per particle, so also four contacts per particle. As the particles are very thin, most of them remain in-plane and out-of-plane effects are negligible. Thus each particle lays on top of two other particles to obtain a stable stacking, so that the average number of contacts per particle becomes 4. Then, as shown in section 1, this corresponds to a compaction $\lambda = 0.5$, so a volume fraction multiplied by 2 from $\overline{\phi}$ and half the thickness than in the bulky state (Eq. (15)) . This hypothesis will be confirmed with the help of physical stacks.

In [5], the authors used numerical simulations to recreate digital composite materials composed of square platelet. They are deposited on a planar domain bounded by vertical walls. In the first step, the platelets are deposited and stacked. As gravity is taken into account, the platelets fall under their own weight and stop when a stable position is found. Next, a mechanical solver is used to compress the resulting material, taking into account particle deformations, mechanical response, and friction between particles. As can be seen in Fig. 5 in [5], different points differ from our assumptions in the initial configuration (after the deposition phase). Along the sidewalls, some platelets deviate from the plane in a region of double the length of

the particle. In the center of the stack, the particles are predominantly in-plane. During the first phase of compression, all particles tend to return to the plane. Similar to our numerical generation, the lower layers seem to be denser than in the rest of the stack, and the upper layers are not full. Also this numerical study is carried out on a single statistical realization. The further comparisons will be done considering the statistical variability quantified from our previous simulations for squared particles, corrected by the multiplicative offset to match the degree of compaction after their numerical deposition under gravity.

From publication data, the thickness after the deposition process is $h_0 = 11$ mm, and the compression velocity is $\dot{h} = -12.2$ mm/s. Platelets are squares of length 12.7 mm and thickness 0.14 mm. 1400 platelets are deposed on a finite domain of dimensions 100 mm x 100 mm. The angular orientation is random and a uniform orientation distribution is considered. The volume fraction after the deposition process is given as $\phi = 31.3\%$. According to Eq. C.1, the bulky volume fraction does not depends of any geometrical parameters and is:

$$\overline{\phi} = \frac{1}{4+\pi} \simeq 14\% \tag{27}$$

Following our assumption for the consolidation under gravitational force, the predicted value for the volume fraction is:

$$\phi_1 = 2\,\overline{\phi} \simeq 28\% \tag{28}$$

As the total thickness is reduced with a constant velocity and the quantity of platelets is conserved, the platelet volume fraction versus time is expressed

as:

$$\phi(t) = \phi_1 \cdot \frac{h_0}{h} = \frac{\phi_1}{1 + \dot{h}t/h_0} \tag{29}$$

Data from Fig.4.b of [5] and values predicted by Eq.29 are compared in Fig.C.10. As the initial platelet volume fraction (ϕ) is slightly different between the publication and the one in Eq.(28) there is an offset between both curves. This initial offset is eliminated in the corrected analytical solution plotted in Fig.C.10, a very good match is obtained up to $\phi = 0.7$. The deviation for $\phi > 0.7$ arises because the platelets become thinner under high mechanical loading. This mechanism is not included in our model where particles are assumed to be infinitely rigid. Nevertheless, the very good match up to $\phi = 0.7$ confirms that our model can be used to describe the deformation in various applications for this class of materials.

4. Results and discussions

The analytical bulky volume fractions (in dot lines) and the average values from the numerical simulations (in black lines) are plotted in ~~Fig.~~ Figs.(C.11-C.14) for different particle shapes. The numerical volume fractions are represented in gray lines for each realizations.

In each case, the numerical estimation of the bulky volume fraction converges toward the analytical value when the number of particles within the stack increases.

As shown in Fig. C.15, the number of particles in the bottom layers (level $z/e = 0$) is generally higher than in the rest of the stack. It is due to the higher probability to stack in the bottom layers, as all particles have to stack first on the bottom plate and then pile up. At the other end, the

top layers which are placed last are incomplete, as the filling of layers is not uniform. The number of particles slowly decreases to zero in the upper layers. In the middle of the stack, the density of particles converges on average to the analytical value Θ. So, most layers are statistically equivalent if there are sufficient number of layers in the stack. Then, the influence of bottom and top boundaries can be neglected. Comparing ~~Fig.~~ Figs.C.11-C.14, the convergence is reached for an areal density higher than 20 particles per unit area (with unit particle length), which corresponds to almost 100 layers in the bulky stack.

The effect of boundaries is important in case of fibers and bundles (enhanced particles). For such cases, the thickness is not well defined, because of unavoidable statistical fluctuations. In such cases, the thickness can be defined with a limit $\Theta/2$. It provides a good estimation of the average thickness to calculate the bulky volume fraction which can be compared to the analytical value.

The comparison with numerical results from [5] show that the proposed statistical model predicts fairly well the platelet volume fraction (ϕ), even in a physical case with gravity effects. Although the analytical model underestimates ϕ by 3% at t=0 (28 % instead of 31 %), it nevertheless gives the correct trend. To further confirm this, predicted values are multiplied by the constant factor of $\frac{31}{28}$ to get the same initial value. As shown in Fig. C.10 a good match is obtained up to the volume fraction of 70%. In [5], the authors explain that they observe small platelet deformations under shear and bending modes until 50%, then deformations by thickness compression arise. Our model shows good agreement and captures the evolution of volume fraction

after important platelet deformations.

To derive the analytical formulas, the assumption of infinite domain must be used. We show in the different bulky simulation that it is sufficient to predict the volume fraction values for enough particles in the stack (an areal density generally equals to at least 20 from Fig. C.14). In the second case, the platelets are stacked in a finite box, so boundary conditions have a certain effect on the stack construction: the local volume fractions are lower along the walls (see Fig. 5 in [5]). Along the upper and lower walls, we explained that the local volume fraction is also different (higher along the lower wall and lower along the upper wall, also see Fig. 5 in [5]). These errors tend to compensate for each other.

Finally, it is noteworthy that authors from [5] simulate only one realization of platelet stack. According to the number of components that they used, the particle density equals to 22.58. The statistical variability can be estimated from Fig. C.14, if we neglect the effect of boundary conditions. Then, the standard deviation is equal to 1.5%. For the stack densified under gravity, we can consider also that this standard deviation is multiplied by 2 (as the average value is multiplied by 2), so an initial standard deviation of 3%. It reveals that our analytical model, without the initial correction, remains in the error interval.

5. Conclusion

Microstructures of randomly distributed particles are ubiquitous and may be represented as a random layered stack of non-cohesive particles. This model material can represent the microstructure of Sheet Molding Com-

pounds or Bulk Molding Compounds. For such cases, the resulting microstructure is mainly influenced by the contacts which induce ~~particle stacking~~ the stacking of the particles. When no ~~loads are~~ load is applied on the stack, the microstructure is ~~referred to as~~ said to be bulky and ~~may~~ can be described ~~with~~ by its bulky volume fraction. This values only depends on the geometrical parameters (particle shape, curvatures and orientation distribution). An equation is derived to obtain an analytical expression of the bulky volume fraction for various particle shapes. This formula is verified by conducting numerical generations of random stacks.

In a general case, a random layered microstructure may be described introducing the compaction as the ratio of the bulky volume fraction to the compacted volume fraction. It leads to a kinematic equation which describes the deformation state of the random microstructure with all internal multi-scale rearrangements of the particles. Such multi-scale transformations are typically present in composite squeeze-flow processes with transport and realignment of particles due to fluid drag forces. Then, the obtained representation addresses the evolution of a population of planar particles with local contact, which gives more geometrical and statistical information about the microstructure than usual continuum approach.This description may be incorporated to generalize mechanical models when considering the mechanical response of the evolving microstructure and its effect on a squeeze-flow, which will be investigated by the authors in future works.

Symbols

A	overlapping area
α	isotropy factor
c	average number of crossings between two particles
e	particle thickness
h	microstructure thickness
$\overline{h}$	bulky thickness
L	fiber length (or particle perimeter)
ℓ	particle length
λ	compaction
N	number of particles
$\vec{p}$	particle orientation vector
ϕ	particle volume fraction
$\overline{\phi}$	bulky volume fraction
ψ	orientation distribution function
r	particle shape factor
ϱ	number of particles per unit area
S	unit area
θ	local orientation
Θ	areal density of particles per layer
v	particle volume
w	particle width

Appendix A. Demonstration of the general formula

The previous proof is based on obtaining equality (8) whatever the angular distribution and the geometry of the particles. To do this, this result should be obtained for a stack of fibers in the general case by showing that the ratio between A and S remains constant.

We start by recalling a relation resulting from the equations (2) and (4) in the case of an isotropic angular distribution:

$$\int \chi d\Gamma = \frac{2}{\pi} \int d\Gamma \tag{A.1}$$

which justifies why the term $2/\pi$ appears in equation (8). More generally, we use the definitions in Eqs (10) and (11), and by introducing the change of variable: $\frac{1}{2\pi}\Gamma^* = \psi\Gamma$ on the configuration space to recover an isotropic configuration, we obtain:

$$Sc = \int \psi\chi d\Gamma = \int \chi \frac{d\Gamma^*}{2\pi} = \frac{2}{\pi} \int \frac{d\Gamma^*}{2\pi} = \frac{2}{\pi} \int \psi d\Gamma = \frac{2}{\pi} Ac \tag{A.2}$$

where we used the relation (A.1). Thus, whatever the stack of fibers, the relation (8) remains true. The quantities Ac and Sc can then be written in the form:

$$Ac = \int \psi\chi d\Gamma = \frac{2}{\pi}\alpha L^2 \tag{A.3}$$

$$Sc = \int \psi d\Gamma = \alpha L^2 \tag{A.4}$$

where we reintroduce the isotropy factor defined in an equivalent way by:

$$\alpha = \frac{\int \psi\chi d\Gamma}{\frac{1}{2\pi}\int \chi d\Gamma} \quad \text{and} \quad \alpha = \frac{\int \psi d\Gamma}{\frac{1}{2\pi}\int d\Gamma} \tag{A.5}$$

Returning to the calculation of (3) in the case of any angular distribution, we obtain a last definition of α given by (9).

To clarify the calculation of (A.2), the change of variable used is equivalent to shearing the configuration by correcting the lengths of the fibers by the isotropy factor to keep them constant. By defining a corrected length: $L^* = \alpha L$, we find the form of the equation (6):

$$\int \psi d\Gamma = \alpha L^2 = \frac{1}{\alpha} L^{*2} = LL^* \tag{A.6}$$

We can also obtain a relation similar to (5) :

$$\int \psi \chi d\Gamma = \frac{2}{\pi} LL^* \tag{A.7}$$

Appendix B. General formulas for integrals on the configuration space

Configuration space:

$$\frac{1}{2\pi} \int d\Gamma = \frac{1}{2\pi} \int d\theta d\ell d\ell' = LL' \tag{B.1}$$

$$\int \psi d\Gamma = \frac{1}{2\pi} \int d\theta d\ell d\ell^* = LL^* \tag{B.2}$$

with $\ell^* = \alpha \ell'$, that we obtain by the change of variable introduced in 5.

Crofton's formula [27]:

$$\frac{1}{2\pi} \int \chi d\Gamma = \frac{1}{2\pi} \int |\sin(\theta)| d\theta d\ell d\ell' = \frac{2}{\pi} LL' \tag{B.3}$$

$$\int \psi\chi d\Gamma = \frac{1}{2\pi}\int |\sin(\theta)| d\theta d\ell d\ell^* = \frac{2}{\pi} L L^* \tag{B.4}$$

with $\int_0^{2\pi} |\sin(\theta)| d\theta = 4$.

Appendix C. Sample calculation

The previous results are applied here to characterize different particle stacks and compute the bulky volume fractions given in [C.1]. The calculations are based on the explicit calculation of A and α as a function of the particles, which gives the other results.

Stack of monodisperse disks: We consider a stack of cylindrical particles, of thin thickness compared to their diameter d. Their axis of symmetry remains vertical in the stack. Two disks intersect if their relative center-to-center distance is less than their diameter. The overlapping surface A therefore draws a disk of radius d. By applying the formula (8), we obtain:

$$S = \frac{\pi^2 d^2}{2} \tag{C.1}$$

This makes it possible to obtain the bulky volume fraction from the definition (7) :

$$\overline{\phi}_{\text{monodisperse}} = \frac{1}{2\pi} \tag{C.2}$$

It is worth to note that the volume fraction is then independent of the parameters of the problem. By applying the definition of α (9) on the circular contours of disks, we trivially obtain that $\alpha = 1$. We deduce the value of c from the bulky volume fraction using (12): $c = 2$, which means that the number of crossings between two circles is equal to 2 (trivial result).

Stack of rectangular particles: We now consider rectangular particles, of length ℓ, width w and thickness e. The thickness is small compared to other dimensions to verify the stack modeling assumptions. We also define the aspect ratio of the particle by $r = \ell/w$.

To describe the angular distribution, it is more convenient to redefine orientation parameters similar to α using the global orientations of the particles and not the local orientations of their outlines. We introduce:

$$\alpha' = \frac{\pi}{2}\langle \|\vec{p} \wedge \vec{p}'\| \rangle \tag{C.3}$$

$$\beta = \frac{\pi}{2}\langle |\vec{p} \cdot \vec{p}'| \rangle \tag{C.4}$$

where $\vec{p}$ and $\vec{p}'$ represent the direction vectors of two different particles (aligned along the length of the rectangular particles). α' measures the isotropy of the distribution. It is equal to 1 for an isotropic distribution in the plane and 0 for aligned particles. Conversely, β' measures particle alignment. It is equal to $\pi/2$ for aligned particles and 1 for isotropic distribution. If we consider the set of configurations with fixed orientations allowing the overlap of two particles, we see that we draw a figure which can be split into 6 zones which can be expressed as a function of α', β', ℓ and w (see Fig. C.16). We thus obtain the overlapping area:

$$A = \frac{2}{\pi}\ell w \left(\alpha' r + 2\beta' + \pi + \alpha' r^{-1}\right) \tag{C.5}$$

Using (8) and (7) the bulky volume fraction of rectangular particles reads:

$$\overline{\phi}_{\text{rectangles}} = \frac{1}{\alpha' r + 2\beta' + \pi + \alpha' r^{-1}} \tag{C.6}$$

One can also analytically calculate the isotropy factor α from its definition (9). For this, we consider the sine of the relative angles of the sides two by two of two particles that we average on the contour. We then obtain:

$$\alpha = \frac{\alpha' r + 2\beta' + \pi + \alpha' r^{-1}}{r + 2 + r^{-1}} \tag{C.7}$$

The average number of crossings between two rectangular contours can then be obtained by (12) :

$$c = 4\left(\frac{\alpha' r + 2\beta' + \alpha' r^{-1}}{\alpha' r + 2\beta' + \pi + \alpha' r^{-1}}\right) \tag{C.8}$$

These results can be simplified for specific configurations. We give the results for aligned rectangles and square particles. In the first case, $\alpha' = 0$ et $\beta' = \pi/2$. In the second case, $\alpha' = 1 = \beta'$ and $r = 1$. The bulky volume fractions are obtained in the two respective cases:

$$\overline{\phi}_{\text{aligned}} = \frac{1}{2\pi} \quad \text{and} \quad \overline{\phi}_{\text{squares}} = \frac{1}{4+\pi} \tag{C.9}$$

Stack of polydisperse disks: Finally, we consider a stack of polydisperse disks. Now the overlapping area A between two particles draws a disk of radius $\frac{1}{4}\langle(d+d')^2\rangle$, where $\langle\cdot\rangle$ denotes the average operator. The calculation of A gives:

$$A = \pi\langle d\rangle^2\left[1 + \frac{1}{2}\frac{\sigma^2}{\langle d\rangle^2}\right] \tag{C.10}$$

with $\langle d\rangle$ the average particle diameter and σ^2 the variance of the diameter distribution. This gives the bulky volume fraction:

$$\overline{\phi}_{\text{polydisperse}} = \frac{1}{2\pi\left[1 + \frac{1}{2}\frac{\sigma^2}{\langle d\rangle^2}\right]} \tag{C.11}$$

References

References

[1] S. J. Pickering, Recycling technologies for thermoset composite materials—current status, Composites Part A: applied science and manufacturing 37 (8) (2006) 1206–1215.

[2] J. Palmer, L. Savage, O. Ghita, K. Evans, Sheet moulding compound (smc) from carbon fibre recyclate, Composites Part A: Applied Science and Manufacturing 41 (9) (2010) 1232–1237.

[3] D. Leblanc, B. Landry, M. Jancik, P. Hubert, Recyclability of randomly-oriented strand thermoplastic composites, ICCM 20 Proceedings.

[4] L. Orgéas, P. J. Dumont, Sheet molding compounds, Wiley Encyclopedia of composites (2011) 1–36.

[5] D. E. Sommer, S. G. Kravchenko, R. B. Pipes, A numerical study of the meso-structure variability in the compaction process of prepreg platelet molded composites, Composites Part A: Applied Science and Manufacturing 138 (2020) 106010.

[6] A. Gibson, S. Toll, Mechanics of the squeeze flow of planar fibre suspensions, Journal of non-newtonian fluid mechanics 82 (1) (1999) 1–24.

[7] C. Servais, J.-A. E. Månson, S. Toll, Fiber–fiber interaction in concentrated suspensions: disperse fibers, Journal of Rheology 43 (4) (1999) 991–1004.

[8] P. Dumont, J.-P. Vassal, L. Orgéas, V. Michaud, D. Favier, J.-A. E. Månson, Processing, characterisation and rheology of transparent concentrated fibre-bundle suspensions, Rheologica acta 46 (5) (2007) 639–651.

[9] G.-P. Picher-Martel, A. Levy, P. Hubert, Compression moulding of carbon/peek randomly-oriented strands composites: A 2d finite element model to predict the squeeze flow behaviour, Composites Part A: Applied Science and Manufacturing 81 (2016) 69–77.

[10] S. Boylan, J. M. Castro, Effect of reinforcement type and length on physical properties, surface quality, and cycle time for sheet molding compound (smc) compression molded parts, Journal of applied polymer science 90 (9) (2003) 2557–2571.

[11] R. Picu, Mechanics of random fiber networks—a review, Soft Matter 7 (15) (2011) 6768–6785.

[12] M. Islam, R. Picu, Effect of network architecture on the mechanical behavior of random fiber networks, Journal of Applied Mechanics 85 (8).

[13] S. Ranganathan, S. Advani, Fiber–fiber interactions in homogeneous flows of nondilute suspensions, Journal of Rheology 35 (8) (1991) 1499–1522.

[14] S. Toll, Packing mechanics of fiber reinforcements, Polymer Engineering & Science 38 (8) (1998) 1337–1350.

[15] W. Nan, Y. Wang, Y. Ge, J. Wang, Effect of shape parameters of fiber on the packing structure, Powder technology 261 (2014) 210–218.

[16] J. Nam, J. Lyu, J. Park, Packing structure analysis of flexible rod particles in terms of aspect ratio, bending stiffness, and surface energy, Powder Technology 357 (2019) 232–239.

[17] C. Van Wyk, 20—note on the compressibility of wool, Journal of the Textile Institute Transactions 37 (12) (1946) T285–T292.

[18] J. Férec, G. Ausias, M. Heuzey, P. Carreau, Modeling fiber interactions in semiconcentrated fiber suspensions, Journal of Rheology 53 (1) (2009) 49–72.

[19] J. Görthofer, M. Schneider, F. Ospald, A. Hrymak, T. Böhlke, Computational homogenization of sheet molding compound composites based on high fidelity representative volume elements, Computational Materials Science 174 (2020) 109456.

[20] S. Fliegener, M. Luke, P. Gumbsch, 3d microstructure modeling of long fiber reinforced thermoplastics, Composites science and technology 104 (2014) 136–145.

[21] S. Deogekar, R. Picu, On the strength of random fiber networks, Journal of the Mechanics and Physics of Solids 116 (2018) 1–16.

[22] A. N. Dickson, K.-A. Ross, D. P. Dowling, Additive manufacturing of woven carbon fibre polymer composites, Composite Structures 206 (2018) 637–643.

[23] M. S. Rizvi, A. Pal, Statistical model for the mechanical behavior of the tissue engineering non-woven fibrous matrices under large deformation,

Journal of the mechanical behavior of biomedical materials 37 (2014) 235–250.

[24] P. Meakin, R. Jullien, Restructuring effects in the rain model for random deposition, journal de Physique 48 (10) (1987) 1651–1662.

[25] M. Nardin, E. Papirer, J. Schultz, Contributional'etude des empilements au hasard de fibres et/ou de particules spheīriques, Powder technology 44 (2) (1985) 131–140.

[26] J. E. Andrade, C. Avila, S. A. Hall, N. Lenoir, G. Viggiani, Multiscale modeling and characterization of granular matter: from grain kinematics to continuum mechanics, Journal of the Mechanics and Physics of Solids 59 (2) (2011) 237–250.

[27] L. A. S. Sors, L. A. Santaló, Integral geometry and geometric probability, Cambridge university press, 2004.

[28] B. Ghanbarian, A. G. Hunt, R. P. Ewing, M. Sahimi, Tortuosity in porous media: a critical review, Soil science society of America journal 77 (5) (2013) 1461–1477.

[29] R. Osserman, The isoperimetric inequality, Bulletin of the American Mathematical Society 84 (6) (1978) 1182–1238.

[30] O. Rahli, L. Tadrist, R. Blanc, Experimental analysis of the porosity of randomly packed rigid fibers, Comptes Rendus de l'Académie des Sciences-Series IIB-Mechanics-Physics-Astronomy 327 (8) (1999) 725–729.

[31] S. G. Advani, C. L. Tucker III, Closure approximations for three-dimensional structure tensors, Journal of Rheology 34 (3) (1990) 367–386.

[32] S. Sultana, A. Asadi, J. Colton, K. Kalaitzidou, Composites made from cf prepreg trim waste tapes using sheet molding compounds (smc) technology: Challenges and potential, Composites Part A: Applied Science and Manufacturing 134 (2020) 105906.

List of Figures

Figure C.1: Carbon Sheet Molding Compounds [32]

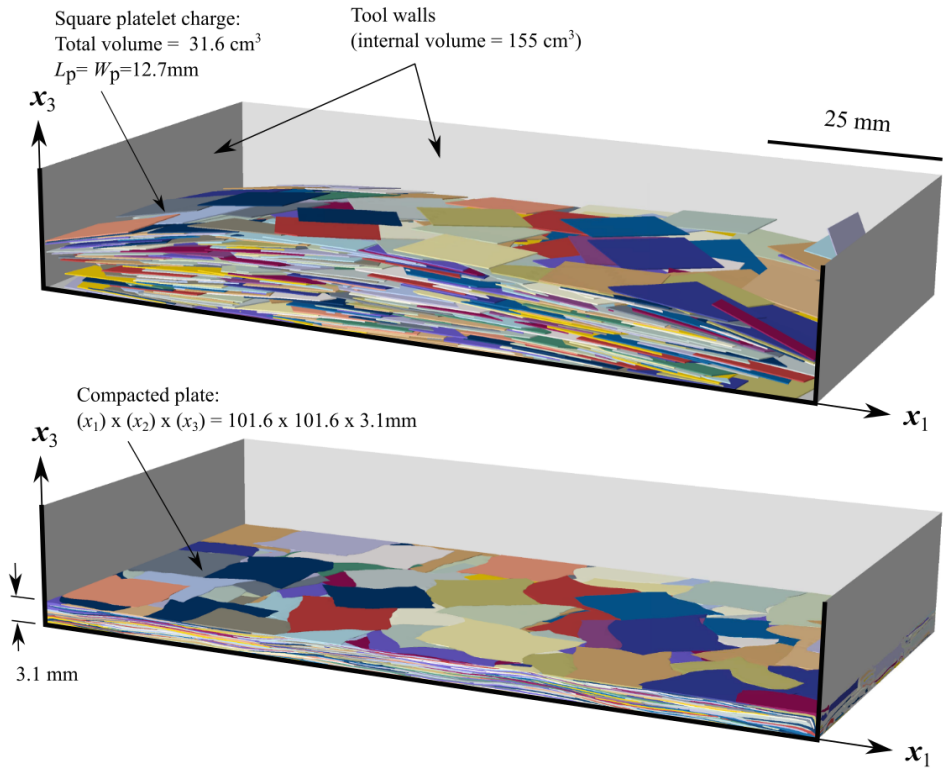

Figure C.2: Numerical deposition of square platelets before and after compaction[5]

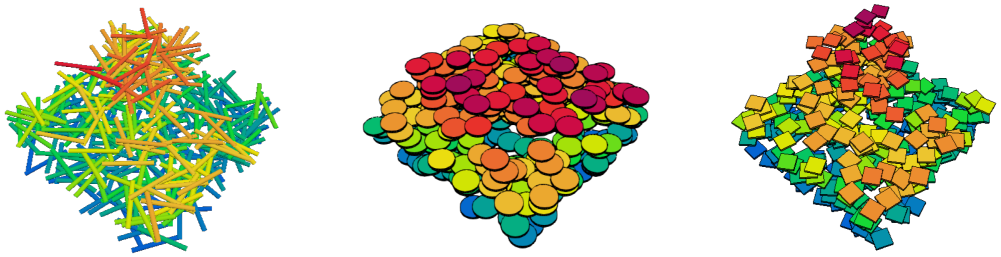

(a) Fiber deposition (b) Disk deposition (c) Square deposition

Figure C.3: Depositions for different particle geometries. Colours represent the location of the layer in the stack in the vertical direction.

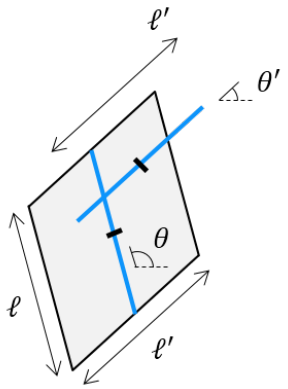

Figure C.4: Overlapping area.

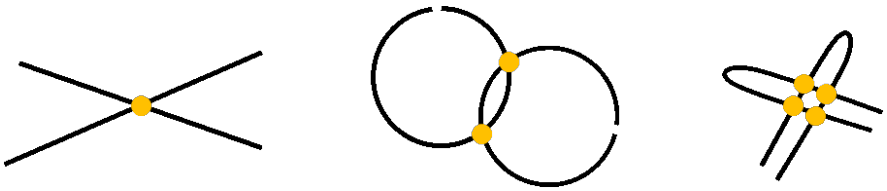

Figure C.5: Number of contacts c for different configurations.

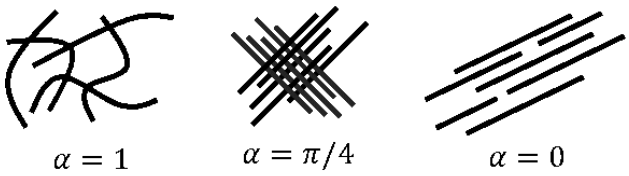

Figure C.6: Values of isotropy factors for different configurations.

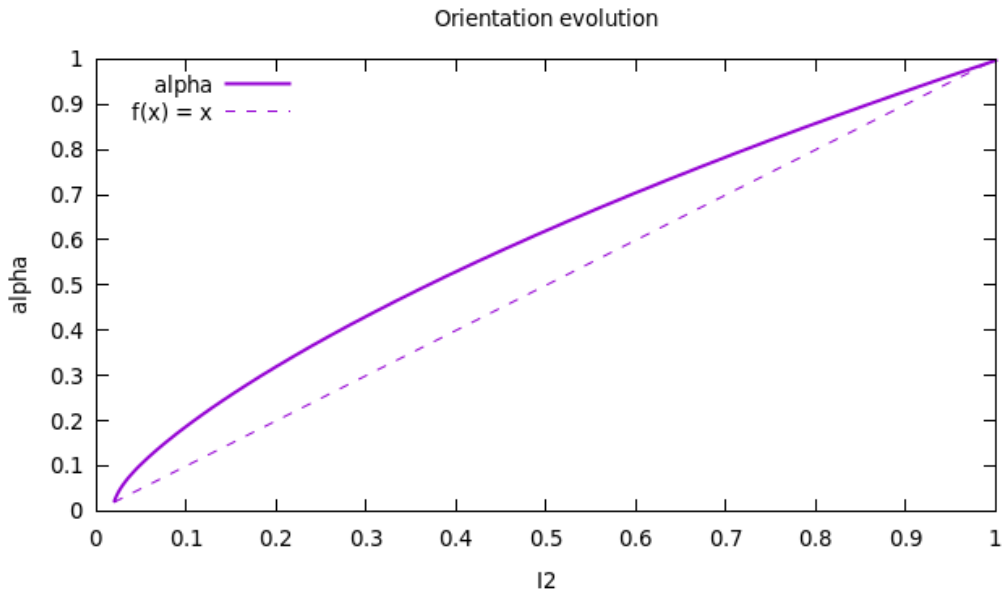

Figure C.7: Isotropy factor α as a function of the second invariant of the orientation tensor A_2

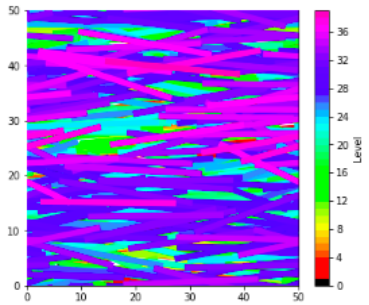

Figure C.8: Top view of a fibrous microstructure with $\alpha = \alpha_{\min}$. Colors represent the altitude of each fiber.

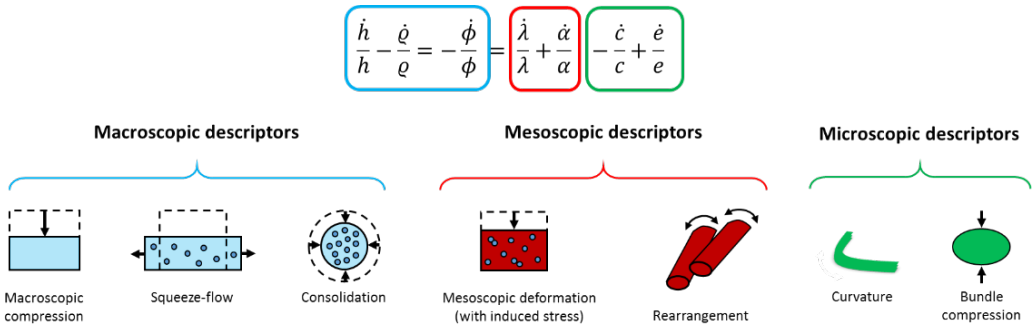

Figure C.9: Multi-scale transformation mechanisms.

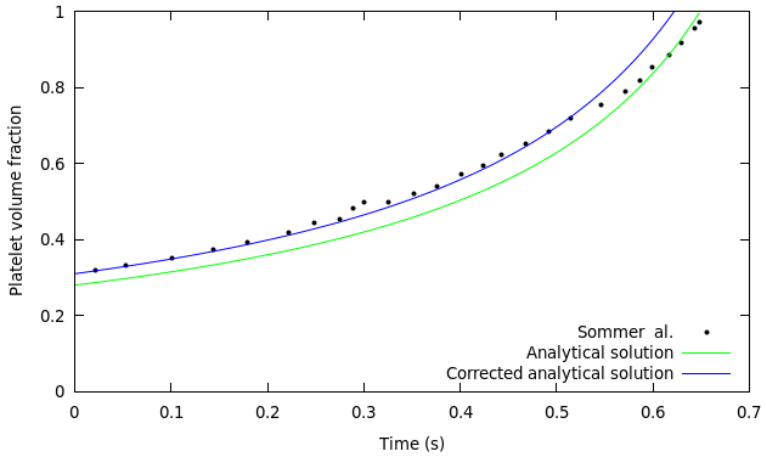

Figure C.10: Comparison between analytical model and numerical simulation from [5]

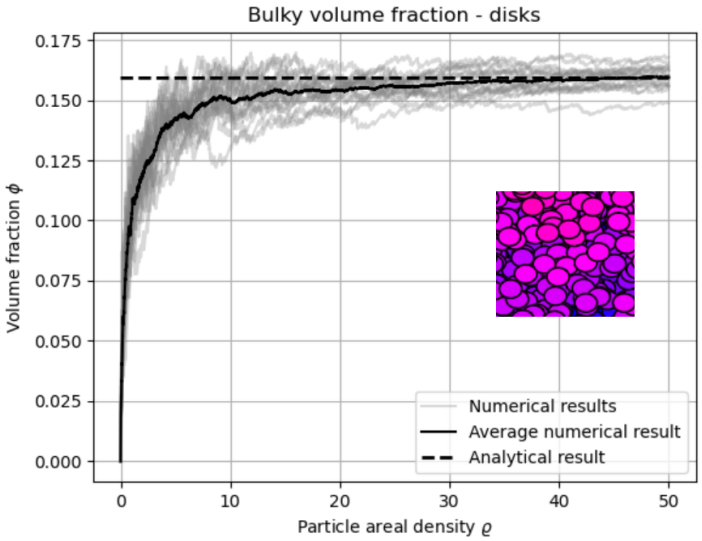

Figure C.11: Distribution of disks.

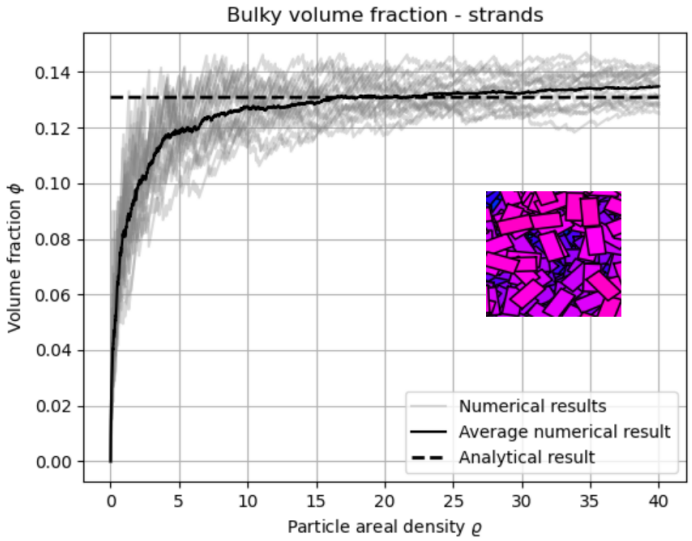

Figure C.12: Isotropic orientation distribution of strands with shape factor $r = 2$.

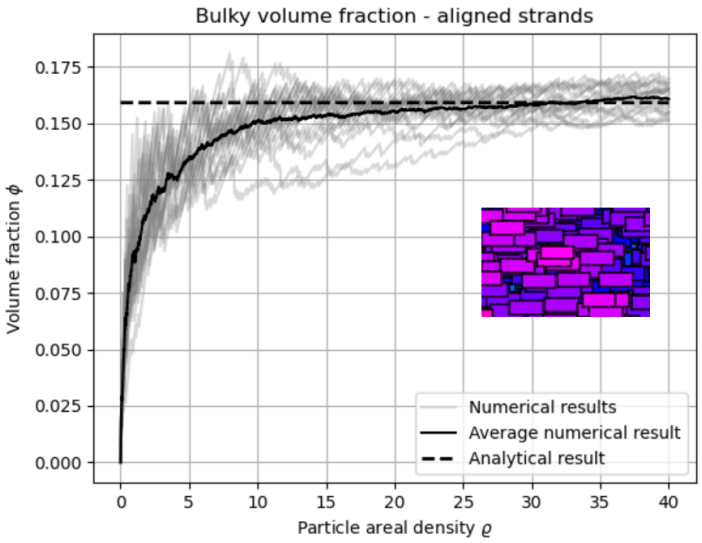

Figure C.13: Distribution of aligned strands ($\alpha' = 0$ and $\beta' = \pi/2$) with a shape factor $r = 2$.

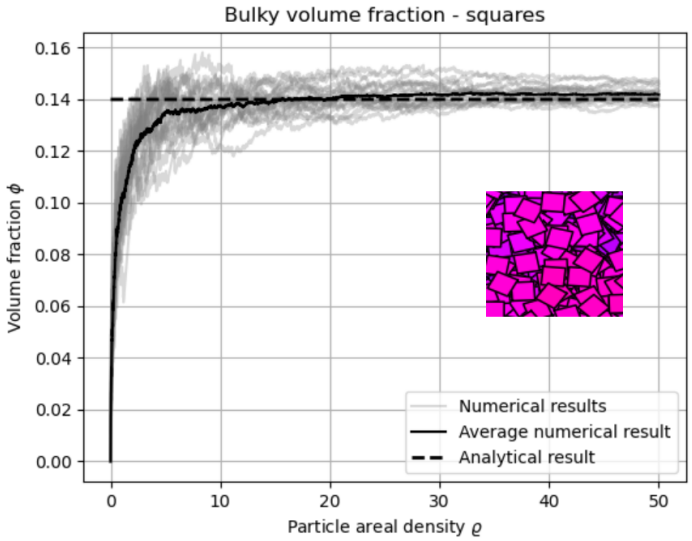

Figure C.14: Distribution of squares.

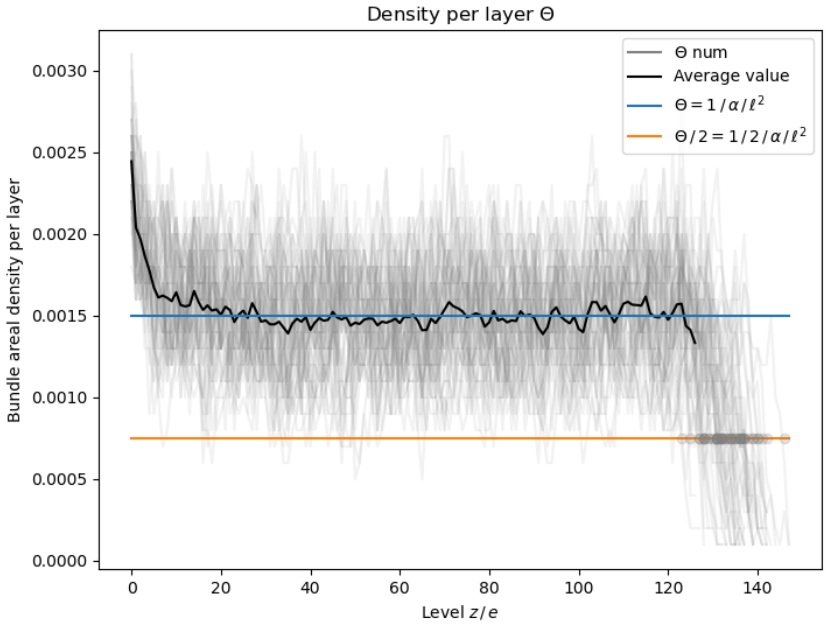

Figure C.15: Density curves through the layers for bundle stacks.

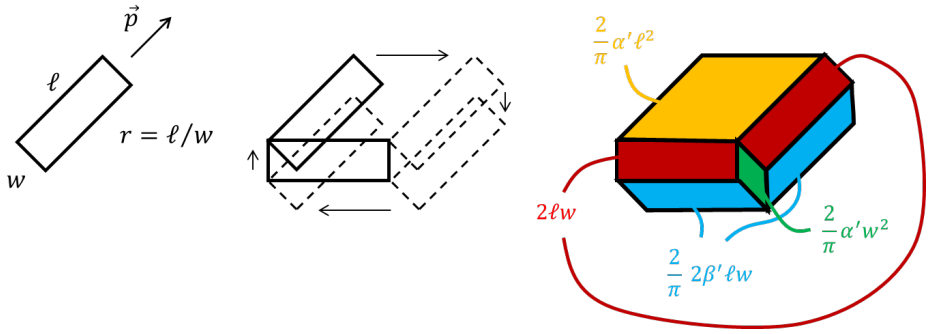

Figure C.16: Overlapping rectangular particles : a) Particle dimensions, b) Construction of the overlapping area, c) Decomposition of the overlapping area.

List of Tables

Particles	Bulky volume fraction $\overline{\phi}$
Fibers	$\frac{cv}{\alpha L^2 e} \propto \frac{c}{\alpha r}$
Disks	$\frac{1}{2\pi}$
Rectangles	$\frac{1}{\alpha' r + 2\beta' + \pi + \alpha' r^{-1}}$
Aligned rectangles	$\frac{1}{2\pi}$
Squares (for $\alpha = 1$)	$\frac{1}{4+\pi}$
Polydisperses disks	$\frac{1}{2\pi(1+\frac{1}{2}(\sigma^2/\langle d\rangle^2))}$

Table C.1: Analytical expression for the bulky volume fraction for different geometrical shaped particles (r is the particle aspect ratio, $\alpha' = \frac{\pi}{2}\langle\|\vec{p}\wedge\vec{p}'\|\rangle$ and $\beta' = \frac{\pi}{2}\langle|\vec{p}\cdot\vec{p}'|\rangle$, where $\vec{p}$ and $\vec{p}'$ are particles' orientation vectors, σ^2 is the variance of the diameter distribution as defined in Appendix B).

Graphical Abstract

A multi-scale statistical description of stacks of non-cohesive thin particles

François Mahé, Christophe Binetruy, Suresh Advani, Julien Férec, Benedikt Eck

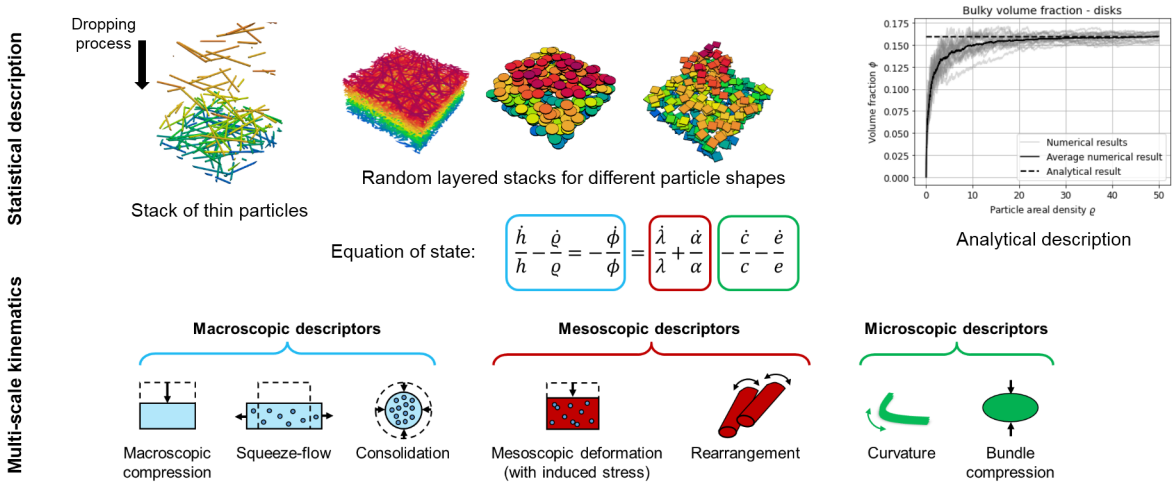

Highlights

A multi-scale statistical description of stacks of non-cohesive thin particles

François Mahé, Christophe Binetruy, Suresh Advani, Julien Férec, Benedikt Eck

- Stacks of non-cohesive thin particles of various shapes
- New multi-scale statistical descriptors
- New analytical equation of state to link geometrical and morphological descriptors
- Uncompressed solid phase volume fractions prediction for different classes of particles
- Generalized deformation measurement for microstructures with internal rearrangements